**Cite as:** Rios, S., Kowalska, M. and Viana da Fonseca, A. (2021). Cyclic and dynamic behavior of sand–rubber and clay-rubber mixtures. Geotechnical and Geological Engineering, DOI:10.1007/s10706-021-01704-3 https://link.springer.com/article/10.1007/s10706-021-01704-3

# CYCLIC AND DYNAMIC BEHAVIOR OF SAND–RUBBER AND CLAY-RUBBER MIXTURES

**Sara Rios**[1]

**Magdalena Kowalska**[2]

**António Viana da Fonseca**[3]

**Key words:** soil-rubber, cyclic triaxial test, damping, stiffness properties, sand, clay

**Contact Address:**

Dr. Sara Rios
Department of Civil Engineering,
Faculdade de Engenharia da Universidade do Porto
R. Dr. Roberto Frias, s/n
4200-465 Porto
*Phone: + 351 225081728*
E-mail: sara.rios@fe.up.pt

Published on 13/2/2021

## ACKNOWLEDGEMENTS

The authors would like to acknowledge BIOSAFE for providing the rubber for this study. This work was financially supported by: Project POCI-01-0145-FEDER-007457 – CONSTRUCT – Institute of R&D in Structures and Construction funded by FEDER funds through COMPETE2020 – Programa Operacional Competitividade e Internacionalização (POCI) – and by national funds through FCT – Fundação para a Ciência e a Tecnologia; Scholarship Reference: SFRH/BPD/85863/2012.

[1] Assistant research fellow and Invited Assistant Professor, CONSTRUCT-GEO, Faculdade de Engenharia (FEUP), Universidade do Porto, R. Dr. Roberto Frias, s/n, 4200-465 Porto, Portugal, sara.rios@fe.up.pt, https://orcid.org/0000-0002-2625-1452

[2] Ph. D., Assistant Professor, Silesian University of Technology (SUT), Department of Geotechnics and Roads, ul. Akademicka 5, 44-100 Gliwice, Poland, magdalena.kowalska@polsl.pl, https://orcid.org/0000-0001-7549-2722

[3] Full Professor, CONSTRUCT-GEO, Faculdade de Engenharia (FEUP), Universidade do Porto, R. Dr. Roberto Frias, s/n, 4200-465 Porto, Portugal, viana@fe.up.pt, https://orcid.org/0000-0002-9896-1410

**ABSTRACT:** In this paper, the possibility of using fine scrap tire rubber to improve the mechanical properties of soil subjected to cyclic loading is addressed. Ground rubber (0.1 - 0.8 mm) in various proportions (0, 9, 33% and 100% by weight) was mixed with a uniform river sand and a lean clay. Cyclic triaxial tests with bender elements were executed to observe the behaviour of the materials and also to determine damping and shear stiffness parameters. The results have shown that the addition of rubber has significantly decreased the density and shear stiffness of both types of soils, which favours mitigation of vibrations. The shear stiffness degradation at shear strains higher than $10^{-3}$ was lower in specimens containing more rubber. Within this strain range, addition of rubber decreased the damping ratio, but increased the normalized accumulated absolute strain energy absorbed by the material. Higher rubber content in sandy specimens resulted in more elastic behaviour, with lower strain accumulation in each loading cycle, eventually resulting in a higher number of loading cycles before failure. The positive effect of rubber presence was not observed in compacted clay-rubber mixture, which sustained less loading cycles than clay alone. The influence of rubber addition in the p'-q stress space was expressed in the form of lower pore pressure generation which shifted the stress path further from the failure envelope.

## 1. INTRODUCTION

Scrap tires are among the largest and most problematic sources of waste. There are several ways to apply this product in civil engineering, reducing the environmental concerns related to their stockpiling or incineration. When scrap tires are shredded they are named tire derived aggregates (TDA). Depending on shape and dimensions, ASTM (2004) distinguishes between powdered rubber (≤ 0.425 mm), ground rubber (≤ 0.425 - 2 mm), granulated rubber (≤ 0.425 - 12 mm), tire chips (12 - 50 mm) and tire shreds (50 – 305 mm).

One of the possible functions the TDA may offer in geo-engineering applications is mitigation of detrimental effects of cyclic loading (stresses or strains oscillating about some equilibrium value) such as increasing settlement or even failure due to liquefaction. The specific type of cyclic loading that presents the most negative impact on people and structures - especially in densely populated areas - is vibrations. They may be characterized with various amplitudes and frequencies depending on the inducing factor: e.g. road and railway traffic, geotechnical works (driving piles, soil compaction), seismic and paraseismic events, such as the ones related with quasi-earthquakes caused by collapse of caverns in deep mining of coal and copper ores. Hence, developing a simple and economical technique for protecting infrastructure against vibrations is important. For this purpose, a useful solution is the isolation of building foundations or retaining walls with cushions filled with TDA or TDA-soil mixtures. This material can be also used to fill open trenches along roads or railways to damp traffic vibrations (Thompson et al. 2016). Such a cushion or a layer works as a distributed isolation system in contrast to conventional systems involving isolation at some discrete supporting points of a foundation. The key advantage of such a geotechnical system is that vibration energy is dissipated already in the ground before it reaches the structure (Tsang et al. 2012). Significant reduction in the potential damage to buildings may be expected in the areas where the soil stiffness is relatively low, resulting in 'moderate to large' strains, and the soil responds nonlinearly (Trifunac 2003). The stiffness reduction can be controlled by rubber content in the TDA-soil mixtures. In order to design the geotechnical vibration isolation adequately, it becomes necessary to evaluate several geotechnical parameters of the considered material, such as its deformation properties (including initial shear modulus $G_0$ and its degradation with strain), damping ratio D, bulk density ρ, Poisson's ratio ν, and shear strength.

Several research works have recently been conducted to study the properties of scrap tires. As described below, most of these studies focused on sand-rubber mixtures with coarse rubber particles. In this research, mixtures of fine ground rubber (< 0.8 mm in size) with sand or clay were studied. The very small size of rubber grains prevented segregation and resulted in greater homogeneity of the mixtures. Another advantage of this fine scrap tire fraction is that, contrary to e.g. chips, it usually does not contain any textile or metal cord, which could affect the properties of the mixture (e.g. possible capillary suction or rusting).

The experimental plan comprised cyclic triaxial tests to determine the evolution of shear modulus G and damping ratio D with shear strain, and bender element tests to estimate the initial values of the shear modulus $G_0$.

## 2. PREVIOUS RESEARCH ON SOIL-RUBBER MIXTURES

Since the 90-ties of XX century several researchers studied the influence of rubber content on the behaviour of sand-rubber mixtures. In most cases the tests considered tire shreds, chips or granulated rubber coarser than 2 mm to be used as embankment fills or retaining wall backfills, insulation or drainage layers, proving the effectiveness of their application both in laboratory and natural scale tests (e.g. Edil and Bosscher 1994; Lee et al. 1999; Yoon et al. 2005; Vinot and Baleshwar 2013, Kowalska and Chmielewski 2017; Chenari et al., 2019). Some researchers proved that smaller chips, crumbs or granules had either no effect on the shear strength of sand or decreased it (Youwai and Bergado 2003, Lee et al. 2007); others, for an optimum rubber content, obtained an increased shear strength at low confining stresses (Ghazavi 2004, Edinçliler et al. 2010, Hong et al. 2015). In the last 20 years, several works have been published on the cyclic and dynamic properties of TDA and TDA-soil mixtures, evaluating dynamic parameters such as shear modulus $G_0$ and damping ratio $D$. Tire chips, shreds and their mixtures with sand or gravel were examined in numerical analyses e.g. by Tsang et al. (2012), Esmaeili et al. (2013), Tsang and Pitilakis (2019), and large-scale laboratory tests by e.g. Hazarika et al. (2008), Gromysz and Kowalska (2017), McCartney et al. (2017). The results proved that this material can effectively reduce vibrations and thus the total (static and dynamic) load applied on structures (etc. quay wall, foundation, road embankment). Although working with different sands and rubber fractions ($D_{50.rubber}/D_{50.soil}$ = 0.2 – 10, where $D_{50}$ is a mean effective grain size), mixture densities and rubber percentages in sand-rubber mixtures, Feng and Sutter (2000), Anastasiadis et al. (2012) and Ehsani et al. (2015) concluded, based on resonant column tests, that an increase in the rubber content caused decrease of the small strain shear modulus $G_0$ and increase of damping ratio $D$. Contrary to the other authors, Nakhaei et al. (2012), while testing well graded gravel with clay mixed with granulated rubber ($D_{50.rubber}/D_{50.soil} \approx 0.4$) in cyclic triaxial tests, observed that the dependency of damping ratio $D$ on rubber content is not unique: although with an increase in rubber inclusion the $D$ increases for the confining pressures of 200 and 300 kPa, it decreases for lower confining pressures of 50 and 100 kPa. Hong et al. (2015) noted that hysteresis loops of the sand-tire rubber mixtures, obtained in cyclic triaxial tests, are more elliptical when compared to the 'butterfly' type of the pure sand loops. Mashiri et al. (2016) indicated that the number of cycles to liquefaction increased with the proportion of tire chips from 10% to 33% and then decreased for 40%.

As mentioned above, there has not been much research done on clay-rubber mixtures and the results are not always in agreement as they depend on the type of soil and dimensions of rubber particles used. According to Tatlisoz et al. (1998) addition of large tire chips decreases the shear strength of clay. It seems, however, that small content of tire buffings, fibres or ground rubber particles may improve the shear strength. Just like in sand-rubber mixtures, rubber addition generally reduces the shear stiffness of clay for both small and large strains. This has been proved by e.g. Özkul and Baykal (2007), Akbulut et al. (2007), Dunham-Friel and Carraro (2011) or Heyer (2012). An exception were the results presented by Akbulut et al. (2007), who obtained higher shear modulus and damping ratio of natural clay after adding small amount of rubber fibres. Apart from the mentioned work by Akbulut et al. (2007), the influence of rubber addition on damping of clay-rubber mixtures has not been investigated.

## 3. TESTING MATERIAL AND PROCEDURES

### 3.1. Soil and rubber properties

Two types of soils were studied: sand and clay, so that the benefit of fine rubber addition could be evaluated for soils that are very different. The sand originated from Coimbra region, in the central Portugal, being a uniform quartz sand from Mondego river. The clay was extracted in Patoka, in the south of Poland, from a mine, belonging to a local brickyard. The mineralogic analysis of the clay made by Stempkowska (2014) revealed that it is composed of quartz, kaolinite, illite, siderite and goethite. Its characteristic red colour results from high amount of iron oxide, while the organic matter content is negligible. It belongs to the tertiary deposits. The clay was oven dried (105°C) and ground in a ball mill to obtain a homogenous and repetitive material for testing.

Table 1 shows the main soil properties and ASTM unified soil classification. Further in the text the soils will be called Red Clay (RC) and Coimbra Sand (CS).

Table 1 around here

The scrap tire rubber of grain dimensions between 0.1 and 0.8 mm was provided by Biosafe (www.biosafe.pt) and it was produced by mechanical shredding of end-of-life tires. According to ASTM (2004) it would be classified as a ground rubber. The physical properties of the rubber are presented in Table 2. In terms of chemical properties, the rubber is composed of polymers (40 to 55%), carbon black (20 to 25%) and other additives. The ground rubber has a grain size distribution similar to the sand (Fig. 1; $D_{50.rubber}/D_{50.sand} = 1.25$), which favours the homogeneity of the moulded sand-rubber specimens and prevents segregation (see Kim and Santamarina, 2008).

Figure 1 around here

Table 2 around here

### 3.2. Specimen preparation and testing procedures

Two sand-rubber mixtures with 9% and 33% rubber content and one clay-rubber mixture with 9% rubber content were prepared. The rubber content ($R$) was defined as the ratio of the dry rubber mass to the total dry mass of the sample (Fig. 2). Additional tests were conducted also for clay-only ($R = 0\%$) and rubber-only specimens ($R = 100\%$). The sand-only behaviour has already been characterized by Teixeira (2015).

Figure 2 around here

The testing program contained cyclic triaxial tests on water saturated specimens, with consolidation and undrained shearing. Two triaxial systems were used: a Bishop-Wesley's 'stress-path cell' and a conventional triaxial cell with rigid connection between the piston and cyclic actuator, enabling cyclic loading with triaxial extension. They are further called: BW cell and CTx cell, correspondingly. Specimens tested in the BW cell were 50 mm in diameter and 100 mm in height and in the CTx cell: 70 mm in diameter and 140 mm in height. The cells were equipped with local strain instrumentation – two axial Hall-Effect transducers (HE) of 5 mm range and bender/extender elements (BE) (Lings and Greening, 2001) in BW cell, and three axial linear variable displacement transformers (LVDTs) in the CTx cell.

Rubber and sand-rubber specimens were prepared in BW cell by moist tamping procedure (see Soares 2015). First, the material was dry mixed until complete homogenization and then small quantity of water was added. It was then gently tamped into the mould in 6 layers. In case of rubber-only specimen this procedure gave higher void ratio due to damping properties of rubber. The sand-rubber mixtures that were to be tested in CTx cell were prepared with slightly greater effort of tamping to get lower void ratios.

The clay and clay-rubber mixture were statically compacted in BW cell in three layers. The moulding water content was about 18%, determined as the optimum water content of the clay in the standard Proctor test giving the maximum dry weight of 17.2 kN/m$^3$ ($\gamma_{d}.^{max}$). The method of static compaction proved satisfactory as the achieved dry weight of the clay specimen was only 1.5% different than the maximum Proctor value. Based on the work by Seda et al. (2007) and Carraro et al. (2013) it was assumed that the optimum water content of the clay-rubber mixtures is the same.

The research program is presented in Table 3, indicating the test name, type of triaxial cell and the used equipment, size of specimen, the calculated specific gravities of the mixtures, together with void ratios and moisture contents of all the specimens. The test names include: the type of soil (CS = Coimbra Sand, RC = Red Clay, R = rubber), rubber content R (0, 9, 33 and 100%) and the effective confining stress $\sigma'_c$; so, a specimen called CS_9_50 represents Coimbra Sand with 9% rubber content by weight sheared at 50 kPa effective confining stress. The specific gravity of each mixture ($G_s^{Mix}$) depends on the rubber content. It can be defined as a function of the specific gravity ($G_s$) and the rubber content R as expressed in Fig. 2.

Table 3 around here

To saturate the rubber and sand-rubber specimens, carbon dioxide was first allowed to percolate through the specimen followed by deaired water percolation. Consequently, saturation was quite fast at a rate of 60 kPa/h. When cell and back pressure achieved 310 and 300 kPa respectively, the Skempton parameter B was measured and values close to 1 were obtained (see Table 3). The clayey specimens were equipped with vertical side drains and water was allowed to percolate for some days before saturation was initiated up to 500 kPa of back pressure at a rate of 20 kPa/h keeping an effective stress of 10 kPa. B values above 0.9 were achieved, which was deemed satisfactory for compacted clays (Black and Lee 1973; Szczepański 2017). Additionally, the P wave propagation time measured at the end of saturation gave P wave velocities close to 1800 m/s, indicating high saturation levels (Vieira, et al., 2005; Jamiolkowski 2012).

All the specimens were consolidated at low confining stress of 50 kPa until the volume change, measured by the amount of water coming out from the specimen, was stabilized (CEN 2004).

The cyclic undrained shearing in BW cell was performed following compression-decompression cycles as expressed schematically in Fig. 3a. The procedure was continued automatically until 20% of permanent axial strain. In this system the loading/unloading velocity was constant being stress-controlled by the deviatoric stress q (the difference between vertical and horizontal stress) at a rate of 2400 kPa/hour, which resulted in decreasing frequency of cycles (Table 4).

The CTx cell was used to perform compression-extension tests on the denser sand-rubber specimens, accordingly to JGS (2000). These tests were performed at a constant frequency of 1 Hz following loading stages (LS) of 10 cycles each, as explained in Table 4 and Fig. 3b. There were 10.5 loading stages applied on each of the two specimens (10 LS + 5 cycles of the $11^{th}$ LS). These tests are indicated by '_CT' at the end of the test name in Table 3.

Figure 3 around here

Table 4 around here

# 4. TEST RESULTS INTERPRETATION

## 4.1. Cyclic tests

The cyclic tests results provide data for analysis of the shear modulus and damping ratio evolution with strain. The shear modulus $G$ is defined as the ratio of the increments of shear stress $\tau$ and shear strain $\gamma$ (see Fig. 4):

$$G = \frac{\Delta\tau}{\Delta\gamma}. \quad [1]$$

Figure 4 around here

Damping ratio $D$ is proportional to the ratio of energy dissipated in one cycle of oscillation $W_D$ and strain energy stored in the system $W_S$ (Kramer, 1996), which can be graphically determined based on a hysteresis loop (see Fig. 4a), using equation:

$$D = \frac{W_D}{4\pi W_S} = \frac{A_{loop}}{4\pi A_\Delta}. \quad [2]$$

In the triaxial tests the area of the loop can be determined as:

$$A_{loop} = \frac{1}{2}\sum_{i=1}^{n}(\tau_i - \tau_{i+1}) \cdot (\gamma_i + \gamma_{i+1}), \quad [3]$$

where $i$ refers to each measurement registered by the system.

The energy absorbed by the material may be evaluated based on the strain energy density, as used by Indraratna et al. (2017) for monotonic shearing. Millen et al. (2019) applied this concept to cyclic tests and suggested normalization by the effective confining stress $\sigma'_c$, calling the obtained parameter *NCASE* (normalized accumulated absolute strain energy). The *NCASE* can be calculated with the following expression:

$$NCASE = \frac{\sum_{j=0}^{n} A_{\Delta}}{\sigma'_c}, j = <0, 1, 2, \dots, n>, \quad [4]$$

where $A_{\Delta}$ is the strain energy equal to the area of the triangle as defined in Fig. 4 and $n$ is the number of peaks in $\tau - \gamma$ graph. Similarly, the normalized dissipated energy of a material (*NDiss*) may be calculated from the area of the loop divided by the effective confining stress $\sigma'_c$, as follows:

$$NDiss = \frac{\sum_{j=0}^{n} A_{loop}}{\sigma'_c}, j = <0, 1, 2, \dots, n>. \quad [5]$$

## 4.2. Bender elements tests

Shear and compression waves propagation time from bender element tests were analysed by the time domain methodology as described by Camacho-Tauta et al. (2015). According to the theory of elasticity, shear wave velocity $V_s$ is related to the shear ($G_0$) modulus, according to equation [6]:

$$G_0 = \rho V_S^2, \quad [6]$$

where $\rho$ is the bulk density of the material. Equation [7] (by Richart et al. 1970) provides the Poisson's ratio value ($\nu$), from which the initial Young's modulus ($E_0$) can be derived [8]:

$$\nu = \frac{0.5\left(\frac{V_P}{V_S}\right)^2 - 1}{\left(\frac{V_P}{V_S}\right)^2 - 1}, \quad [7]$$

$$E_0 = 2G_0(1 + \nu). \quad [8]$$

# 5. RESULTS AND DISCUSSION

## 5.1. Stress-strain relations and stress paths in compression-decompression cyclic tests

The number of loading stages that each specimen tested in compression-decompression sustained before failure is presented in Table 5. The failure was defined as an achievement of an accumulated axial strain of 20%.

Table 5 around here

The results of the cyclic compression-decompression tests in the form of shearing characteristics $\tau - \gamma$ (loops) are presented in Fig. 5 for sand-rubber mixtures and in Fig. 6 for clay-rubber mixtures. The rubber alone test was repeated in both figures to serve as a reference. The last loading stage (usually incomplete) is marked by grey colour. The graphs are shown in semi-logarithmic scale so that more loading stages could be observed despite the different strain levels.

Figure 5 and 6

When the boundaries of $\tau - \gamma$ are compared (dashed lines in Fig. 5 and Fig. 6) it may be noticed that the increase in the rubber content leads generally to decrease of the shear stiffness, although this influence takes different forms in sandy and clayey specimens.

Looking at Fig. 5c, it is clear that the $\tau - \gamma$ envelope of CS_9_50 specimen shows initially lower shear strains than CS_33_50 specimen, but starting from the shear strains of about 0.065 this tendency gets reversed, which is even better expressed in the R_100_50 test, which sustained the highest number of loading stages before reaching 20% axial strain. The $\tau - \gamma$ envelopes of CS_33_50 and R_100_50 specimens initially coincide, which means that addition of 33% of rubber by weight (53% by volume) changes the behaviour of the sandy specimen into more rubber-like. A similar coincidence is visible in generation of pore pressure - see Fig. 9a. According to Lee et al. (2007) a specimen with this rubber content corresponds to a transition mixture, which can show either sand- or rubber-like behaviour depending on the value of confining stress - at the small confining stress of $\sigma'_c$ = 50 kPa the mixture is expected to behave in a rubber-like mode, which has been proved also in this research. It may be noticed that the behaviour of the sandy specimen containing more rubber is more elastic. Looking for example at the results for the 5th loading stage of the specimen CS_33_50: all the loops $\tau - \gamma$ follow the same hysteretic loop, while in case of the specimen CS_9_50 (with less rubber content) the strain tends to accumulate in each cycle. As a result, before 20% axial strain, the CS_33_50 specimen is able to sustain more loading stages than CS_9_50 (Table 5). The specimen R_100_50 shows smaller strain accumulation in each single loading stage sustaining 7 full loading stages up to the end of the test. It might be noted that the positive influence of rubber addition in sand-rubber mixtures was activated in the 5th LS at about 10% of axial strain, when the accumulated strain became lower for R = 33% than for R = 9%. The reason is probably the mobilization of elastic deformation of rubber grains in compression.

From the tests performed with clay (Fig. 6 a, b) it can be observed that introduction of 9% of rubber by weight did not improve the soil behaviour. The specimen RC_9_50 sustained less cycles than clay-only specimen, indicating that even such a relatively small rubber content may drastically change the behaviour of compacted clay. The rubber grains in the compacted clay-rubber mixture got less deformed than in the sand-rubber specimen with the same rubber content and so the elastic properties of rubber could have not been fully utilized. This observation, however, needs further studies on clay samples with other rubber contents.

The effective stress paths p' – q obtained in compression-decompression tests are presented in Fig. 7 and Fig. 8. The colourful dashed lines represent the possible peak shear strength boundaries if assumed that they pass through the origin. In Fig. 7 the boundary of Coimbra Sand obtained by Teixeira (2015) (CS_0) has been also added for comparison. It may be noticed that the shear strength of sand gets increased when 9% rubber is added to the mixture, but the effect becomes lower at 33% rubber content. From these results, it seems that the optimum rubber content in sand-rubber mixture would be around 9%. However, more tests are needed to confirm this. In case of clay, 9% rubber addition decreases the shear strength slightly. The highest shear strength has been obtained for the rubber-alone specimen, which corresponds with the highest number of loading stages applied before 20% axial strain.

Figure 7 and 8

The positive effect of rubber addition seems to result from generation of lower excess pore pressures (Δu) (see Fig. 9), which shifts the effective stress paths further from the failure boundary making space for another loading stage. For axial strains up to 10% the maximum Δu is smaller in the CS_33_50 than in the CS_9_50 and also smaller in the RC_9_50 than in the RC_0_50 specimen, with the lowest values in the R_100_50. The compressive energy is used to deform the specimen rather than to build the excess pore pressure in the undrained test. Interestingly, the fluctuations of pore pressure in one loading stage are the greatest in clay and the smallest in sand, with the average values in rubber-only specimen. The maximum excess pore pressure in rubber-only specimen is constantly growing till the end of the test and so eventually, before failure, it overcomes the pore pressure in sandy and clayey specimens.

The fact that the increased rubber content caused the decrease in excess pore pressure may be surprising if compared with literature. For example, Shariatmadari et al. (2018), testing Firouzkooh sand mixed with rubber granulate (1 – 2 mm in size), obtained a clear decrease of excess pore pressure in undrained monotonic loading for mixtures containing more rubber. This difference may be explained by the fact that the specimens tested by Shariatmadari et al. (2018) were all prepared with the constant relative density of about $D_r$ = 54.5%, while the specimens prepared in this study were prepared with constant tamping effort. Considering that the addition of rubber to sand increases both the $e_{max}$ and $e_{min}$ values (see e.g. Madhusudhan et al. 2017, Shariatmadari et al. 2018), the similar void ratios of 0.88 and 0.86 in CS_9_50 and CS_33_50 specimens, respectively, correspond to different $D_r$ values, with CS_33_50 specimen being relatively denser and thus less compressive than CS_9_50. The effect of decreased excess pore pressure at higher rubber content seems to be dependent on the material state, given by not only its density, but also the confining pressure. This may be supported by the results of research conducted by Ozkul and Baykal (2007), where at 100 kPa of confining pressure, lower values of Δu were reported for specimens with 10% rubber buffings content than for specimens with no rubber; while at higher confining pressures (200 & 300 kPa) the opposite trend was observed. This is also in agreement with the liquefaction study by Mashiri et al. (2016) on loose sand-rubber mixtures, in which at 69 kPa of confining stress an increasing number of cycles was obtained for increasing amount of rubber (10 – 30%).

Figure 9 around here

## 5.2. Stress-strain relations in compression-extension cyclic tests on sand-rubber mixtures

The results of compression-extension cyclic tests performed on the denser sand-rubber specimens in the form of stress-strain loops $\tau - \gamma$ and stress paths $p' - q$ are presented in Fig. 10 and Fig. 11, respectively.

Figure 10 and 11 around here

It may be noticed that the τ – γ loops of the test with lower percentage of rubber (CS_9_50_CT) show a “butterfly” shape starting from the 10th loading stage. Their tangent shear stiffness modulus during reloading is initially quite high, then it drops as the q value is reaching zero and raises again at higher absolute values of q, which is commonly observed for pure sands at higher cyclic stress ratios (CSR = $q/2\sigma'_c$; here at 10$^{th}$ LS: CSR =

0.35) (see e.g. Kumar et al., 2015). The loops of the test with higher rubber percentage are more elliptical, showing no increase of tangent shear stiffness modulus in reloading. This has also been observed by Hong et al. (2015) as indication of the visco-elastic influence of rubber. It is also clear that accumulation of $\Delta\gamma$ with each cycle is higher in the case of the specimen containing less rubber grains – see e.g. the 10th loading stage: in CS_9_50_CT test $\Delta\gamma$ increased from 0.02 in the 1st cycle to 0.06 in the 10th cycle and in CS_33_50_CT test: from 0.05 to 0.06 respectively. As the result, even though the shear strain increase ($\Delta\gamma$) is initially (in the first loading stages) lower for the CS_9_50_CT specimen, it becomes eventually similar to the one for CS_33_50_CT specimen as the number of loops increases. This behaviour is consistent with the one observed in compression-decompression tests on the looser specimens.

It is also clear that the $\tau - \gamma$ loops are not symmetrical with reference to the vertical axis – the absolute strain values are higher in triaxial extension than in triaxial compression. This is most visible in the last loading stage (represented in grey), where the specimen is approaching failure. Also, the shapes of the stress paths are non-symmetrical in reference to the p' axis – they show smaller shear stress in triaxial extension than in compression. It shall be noted, that the CT tests were finished without reaching failure, thus the stress paths cannot be used to determine the actual positions of the failure envelopes. Even though, the results seem to indicate that the failure surface of the sand-rubber mixtures is nonsymmetrical against hydrostatic axis with lower shear strength in triaxial extension than compression – being consistent with the Coulomb-Mohr failure criterion for soils as demonstrated on sandy specimens by e.g. Yamada and Ishihara (1979) or Ishihara (1985).

If the shapes of the stress paths are compared (to make it easier the boundary of the stress path of one specimen was copied on the stress path of the other – dashed lines in Fig. 11), it can be noted that the specimen CS_9_50_CT has achieved lower mean effective stress (p') after 10.5 loading stages - due to higher pore pressure generation in comparison with CS_33_50_CT. This pattern is similar to the one observed in compression-decompression tests, indicating that the rubber may help in reduction of excess pore pressure. The evolution of the excess pore pressure $\Delta u$ with strain obtained in the first 10 loading stages of compression – extension tests is presented in Fig. 12.

Figure 12 around here

### 5.3. Stiffness and damping properties

Results of the bender element tests are presented in Table 6, summarizing P and S wave velocities (measured at the end of consolidation) and corresponding elastic stiffness properties. For comparison the results of clean Coimbra Sand obtained by Teixeira (2015) were added – specimen called CS_0_50.

Table 6 around here

It is clear from Table 6 that the increase of the rubber content resulted in a decrease of $E_0$ and $G_0$, which is consistent with the results obtained by other researchers (Feng and Sutter, 2000, Dunham-Friel and Carraro, 2011 or Anastasiadis et al., 2012). The dependency of shear stiffness on rubber content is not linear: addition of 9% of rubber by weight to sand had a negligible influence on the maximum shear stiffness, while for R = 33% it showed a drop as high as 77%. The effect of rubber addition on clay stiffness is very high already at R = 9%, giving a $G_0$ value 58% lower than for clean clay.

The P wave velocities in all specimens were higher than 1450 m/s, giving Poisson ratio's values very close to 0.5. These results prove proper saturation of the specimens. According to Valle Molina and Stokoe (2012), Jamiolkowski (2012), or Ghasemzadeh and Abounouri (2013) P wave velocity in soil increases rapidly when saturation ratio S is higher than 0.95.

The normalized shear moduli ($G/G_0$) versus the shear strain amplitude $\Delta\gamma/2$ (see Fig. 4) are presented in Fig. 13 together with the boundaries proposed by Mashiri et al. (2016) for mixtures containing 0 – 40% of tire chips (up to 8 mm in size). The G values were calculated based on the 5th out of 10 cycles in each loading stage. The $G_0$ points have been located at shear strains equal to $10^{-5}$ being the range applied in bender elements tests according to Dyvik and Madshus (1985). The CTx cell was not equipped with bender elements that is why the $G_0$ values in compression-extension tests could have not been obtained directly. They were assessed as the slope of the initial tangent of the $\tau$ - $\gamma$ graph on the reloading part. The values: $G_0$ = 50 MPa and 11 MPa were obtained in CS_9_50_CT and CS_33_50_CT tests, respectively, being greater than the $G_0$ values in the CS_9_50 and CS_33_50 tests due to their higher density.

As expected, the shear stiffness values show continuous decrease with strain, which proves the nonlinear behaviour of soil-rubber mixtures. The compression-extension tests gave higher shear stiffness values than compression-decompression tests, due to higher specimens' density and also as the result of faster strain rates, as reported by Watanabe and Kusakabe (2013). It is evident that at larger shear strains the degradation of shear stiffness in rubber-only specimen is much smaller than in all other mixtures and clay, being the effect of elastic properties of rubber. This is in agreement with other researchers (e.g. Nakhaei et al., 2012) who report a smaller stiffness degradation with increased rubber content. In case of sand-rubber mixtures addition of rubber makes the stiffness degradation smaller starting from strains greater than about $4 \cdot 10^{-4}$, independently of the test type . In clay-rubber specimen, this effect is visible at larger strain range – starting from about $6 \cdot 10^{-3}$. The results fit quite well to the boundaries obtained by Mashiri et al. (2016) only for strains larger than $5 \cdot 10^{-4}$. The reason for this may be the fact that the boundaries were defined based on other types of tests (resonant columns and hollow cylinder), which are more accurate than cyclic triaxial at very small strains.

Figure 13 around here

It is well known that during a cyclic loading the soil damping tends to increase due to soil yielding and consequent increase in deformation (e.g. Kokusho, 1980, Ishibashi and Zhang, 1993). The damping ratios of all the mixtures at confining pressure 50 kPa are presented in Fig. 14 together with the boundaries proposed by Mashiri et al. (2016) and by Madhusudhan et al. (2017). , It was not possible to provide reliable damping ratios for very small shear strain (below $10^{-4}$), due to insufficient precision of strain measurements in cyclic triaxial tests, which would be interesting for many vibration purposes. The results of the current research match well with the results of Mashiri et al. (2016) for strains smaller than $10^{-3}$ and with the results of Madhusudhan et al. (2017) in the higher strain range. The difference may be connected with the size of rubber particles tested – Mashiri et al. (2016) used bigger rubber chips, while Madhusudhan et al. (2017) worked on material similar to the one used in this research (see Table 7).

Figure 14 around here

The addition of fine ground rubber decreases the damping ratio of Coimbra Sand and Red Clay. This agrees with the results of cyclic triaxial tests obtained by other authors (Nakhaei et al. 2012, Pistolas et al. 2018, Madhusudhan et al. 2018, 2019), contrary to the results of resonant column tests (Anastasiadis et al. 2012, Pistolas et al. 2018), in which much smaller strain range is applied. A comparison of results of resonant column and cyclic triaxial tests obtained by several authors for various sand-rubber mixtures can be found in Table 7. This may be explained by large difference between the initial stiffnesses of soil and rubber at very low strains, which becomes smaller for larger strains, and by high elastic deformation capacity of rubber grains at low confining pressures. The influence of confining stress on damping ratio was explained by Nakhaei et al. (2012) – at high rubber content the mixture exhibits more plastic strain at high confining pressures and more elastic strain at low confining pressures.

Table 7 around here

The values of the normalized cumulative absolute strain energy (NCASE), as defined in equation (4), and the normalized dissipated energy, as defined in equation (5), are presented in Fig. 15 and Fig. 16 against the number of cycles. It shall be noted that in compression-decompression and compression-extension tests there were different amplitudes and different numbers of cycles applied, so the results can be only compared within the same type of test.

Although the amount of energy dissipated in one loading cycle is increasing (Fig. 16), the strain energy stored in the system ($A_\Delta$ - see equation (2) and Fig. 4) is increasing faster (Fig. 15), and therefore the damping decreases. Higher NCASE values indicate better absorbing properties and high ductility of rubber particles, which is in agreement with the previous observations about the effect of rubber on the resilience of the mixtures as reported by Indraratna et al. (2017) for monotonic tests. The reduction of D is not down to zero as rubber shows a minimum value, equal to about 8%. Almost the same value has been obtained in cyclic triaxial tests on scrap tire chips by Mashiri et al. (2016) and Madhusudhan et al. (2019). The damping curve of rubber-only specimen shows a decrease of D for shear strains between $10^{-3}$ to $10^{-2}$ and a slight increase for higher strains. A similar parabolic shape of the damping curve was presented by McCartney et al. (2017) for their cyclic simple shear tests on large (up to 300 mm in size) tire chips.

Figures 15 and 16 around here

## 6. CONCLUSIONS

The compression-decompression tests on clay, clay-rubber and sand-rubber mixtures and compression-extension tests on sand-rubber mixtures at 50 kPa confining pressure led to the following conclusions:

1) introduction of rubber reduced pore pressure build-up in all the tested mixtures, although this effect seems to be valid only for low confining pressures; for sandy specimens this may be explained by the fact that at similar void ratio the specimen with higher rubber content has higher relative density and so its dilation increases;

2) the sand-rubber specimen containing 33% rubber by weight exhibited more elastic behaviour and much less accumulation of strain in cyclic compression-decompression loading than the specimen with lower rubber content - the positive influence of rubber was activated in the 5$^{th}$ LS at about 10% of axial strain, probably due to mobilization of elastic deformation of rubber grains in compression;
3) the positive effect of increased number of LS at higher rubber content, that was noticed in sand, was not present in the clay-rubber mixture, as lower strains did not mobilize the elastic properties of rubber;
4) the peak shear strength of sand can be increased when rubber is added, being this increase higher with 9% rubber content than with 33% rubber content. On the contrary, 9% rubber content in compacted clay specimen decreases the shear strength in relation to the clay alone;
5) addition of rubber significantly decreases the initial soil stiffness moduli $G_0$ and $E_0$;
6) the shear stiffness values show constant decrease with strain; the degradation of shear stiffness in rubber-only specimen is much smaller at larger shear strains than in all the other mixtures and clay, being the effect of elastic properties of rubber;
7) the addition of rubber to soil reduced the damping ratio $D$ towards the minimum value of about 8% at the shear strain amplitude of 1% - this trend seems to be characteristic for mixtures tested in cyclic triaxial tests, where shear strains greater than $10^{-4}$ can be analysed;
8) the addition of highly ductile rubber crumbs causes an increase of the normalized accumulated absolute strain energy *NCASE*, leading to an enhanced energy-absorbing capacity of the mixture.

The above results indicate that the use of very small (ground) rubber particles leads to a significant reduction in stiffness for both high strains (evaluated in cyclic triaxial tests) and low strains (evaluated by bender element measurements). This is consistent for both loose and compacted sand, as well as for clay-rubber mixture. As demonstrated by Tsang et al (2010) this reduction in stiffness can retard the accelerations transmitted to the structures. However, at shear strains greater than $10^{-4}$ the damping ratio seems to reduce with increasing rubber content, conversely to what can be found for smaller strains in resonant column tests – this reduces the effectiveness of mixing the finest rubber fraction with soil as a damping material when higher amplitudes of cyclic loading are expected.

## REFERENCES

Akbulut S, Arasan S, Kalkan E (2007) Modification of clayey soils using scrap tire rubber and synthetic fibers. Applied Clay Science, 38:23–32

Anastasiadis A, Senetakis K, Pitilakis K (2012) Small-strain shear modulus and damping ratio of sand-rubber and gravel-rubber mixtures. Geotech Geol Eng 30(2):363-382

ASTM (ASTM International) (2004) Standard Practice for Use of Scrap Tires in Civil Engineering Applications, D 6270 – 98, Vol. 11.04

ASTM (ASTM International) (2010) Standard Test Method for Metal Powder Specific Surface Area by Physical Adsorption. B 922, Vol. 02.05

ASTM (ASTM International) (2011) Standard Practice for Classification of Soils for Engineering Purposes (Unified Soil Classification System). D 2487 – 11, Vol. 04.08

ASTM (ASTM International) (2016) Standard Test Methods for Maximum Index Density and Unit Weight of Soils Using a Vibratory Table, D 4253 – 16, Vol. 04.08

ASTM (ASTM International) (2016a) Standard Test Methods for Minimum Index Density and Unit Weight of Soils and Calculation of Relative Density, D 4254 – 16, Vol. 04.08

ASTM (ASTM International) (2012) Standard Test Method for True Specific Gravity of Refractory Materials by Gas-Comparison Pycnometer, C604-02

Black DK, Lee KL (1973) Saturating laboratory samples by back pressure. Journal of Soil Mechanics and Foundations Division, ASCE 99, No. SM1:75-93.

Camacho-Tauta J, Cascante G, Viana da Fonseca A, Santos JA (2015) Time and frequency domain evaluation of bender elements systems. Geotechnique, 65(7):548-562

Carraro A, Budagher E, Badanagki M, Kang JB (2013) Sustainable Stabilization of Sulfate-Bearing Soil with Expansive Soil-Rubber Technology. Technical Report No. CDOT-2013-2, March 2013

CEN (2004) ISO/TS 17892-9:2004 Geotechnical investigation and testing – Laboratory testing of soil: Consolidated triaxial compression tests on water saturated soil. Brussels

CEN (2009) ISO/TS 17892-12:2009. Geotechnical investigation and testing - Laboratory testing of soil - Part 12: Determination of Atterberg limits. Brussels

CEN (2010) TS 14243-Materials produced from end of life tires. Specification of categories based on their dimension(s) and impurities and methods for determining their dimension(s) and impurities. Brussels

Chenari JR, Alaie R, Fatahi B (2019) Constrained Compression Models for Tire-Derived Aggregate-Sand Mixtures Using Enhanced Large Scale Oedometer Testing Apparatus. Geotech Geol Eng 37, 2591-2610. https://doi.org/10.1007/s10706-018-00780-2

Dunham-Friel J, Carraro JAH (2011) Shear Strength and Stiffness of Expansive Soil and Rubber (ESR) Mixtures in Undrained Axisymmetric Compression. American Society of Civil Engineers, Geotechnical Special Publication, (211 GSP), 1111–1120. doi:10.1061/41165(397)114

Dyvik R, Madshus C, (1985) Lab measurements of $G_{max}$ using bender elements. Proceedings ASCE Annual Convention: Advances in the art of testing soils under cyclic conditions, Detroit, Michigan, 1985:186–197.

Edil TB, Bosscher P J (1994) Engineering properties of tire chips and soil mixtures. Geotech. Testing J., 17(4):453–464

Ehsani M, Shariatmadari N, Mirhosseini SM (2015) Shear modulus and damping ratio of sand-granulated rubber mixtures. Journal of Central South University, 22(8):3159–3167

Edinçliler A, Baykal G, Saygili A (2010) Influence of different processing techniques on mechanical properties of used tires in embankment construction. Waste Management, 30:1073-108

Esmaeili M, Mosayebi SA, Nakhaee N (2013) Performance of Shred Tire Mixed with Railway Subgrade in Reduction of Train Induced Vibrations. Adv. Railw. Eng. Int. J. 1(1):37–49.

Feng ZY, Sutter KG (2000) Dynamic properties of granulated rubber-sand mixtures. Geotech. Test. J., GTJODJ, 23(3), September:338-344.

Ghasemzadeh H, Abounouri AA. (2013) Compressional and shear wave intrinsic attenuation and velocity in partially saturated soils. Soil Dyn Earthq Eng, 51:1–8. doi:10.1016/j.soildyn.2013.03.011.

Ghazavi M (2004) Shear strength characteristics of sand-mixed with granular rubber. Geotech. and Geol. Eng., 22:401-416.

Gromysz K, Kowalska M (2017) Reduction of vibrations applied on structures - results of chamber tests with the use of tire derived aggregate. Procedia Eng., 193:305–312

Hazarika H, Kohama E, Sugano T (2008) Underwater Shake Table Tests on Waterfront Structures Protected with Tire Chips Cushion. J. Geot. Geoenv. Eng.,134(12):1706–1719

Heyer NC (2012) Swell, stiffness and strength of expansive soil-rubber (ESR) mixtures at various scales: effect of specimen and rubber particle sizes. MSc thesis, Colorado State University, Fort Collins

Hong Y, Yang Z, Orense RP, Lu Y (2015) Investigation of Sand-Tire Mixtures as Liquefaction Remedial Measure. Proc. 10th Pacific Conf. on Earthq. Eng. - Building an Earthq. Resilient Pacific, Australian Earthq. Eng. Society, Sydney, Australia.

Indraratna B, Qi Y, Heitor A (2017) Evaluating the Properties of Mixtures of Steel Furnace Slag, Coal Wash, and Rubber Crumbs Used as Subballast. J. Mater. Civ. Eng., 2018, 30(1):04017251

Ishibashi I, Zhang X (1993) Unified dynamic shear moduli and damping ratios of sand and clay. Soils and Foundations, 33(1):182-191.

Ishihara K. (1985) Stability of natural deposits during earthquakes. Proc. 11th Int. Conf. on Soil Mech. and Found. Eng., San Fransisco: Balkema:321–376.

ISO (2004) 14688-2 Geotechnical investigation and testing. Identification and classification of soil. Part 2: Principles for a classification.

ISO (2015). 60 Plastics. Determination of apparent density of material that can be poured from a specified funnel.

Jamiolkowski M (2012) Role of geophysical testing in geotechnical site characterization. Victor de Mello Lecture, São Paulo. Soils and Rocks, 35(2):117-137

JGS (Japanese Geotechnical Society) (2000) Method for cyclic triaxial test to determine deformation properties of geomaterials. JGS 0542-2000

Kim H-K, Santamarina JC (2008) Sand-rubber mixtures (large rubber chips). Can. Geot. J., 45:1457-1466

Kokusho T (1980) Cyclic triaxial test of dynamic soil properties for wide strain range. Soils and Foundations, 20(2):45-60.

Kowalska M, Chmielewski M (2017) Mechanical Parameters of Rubber-Sand Mixtures for Numerical Analysis of a Road Embankment. WMCAUS - IOP Conf. Series: Materials Science and Eng., 245 (2017) 052003 doi:10.1088/1757-899X/245/5/052003

Kramer SL (1996) Geotechnical Earthquake Engineering. Pearson, Upper Saddle River, N.J.

Kumar SS, Krishna AM, Dey A (2015) Cyclic response of sand using stress controlled cyclic triaxial tests. Proc. 50th Indian Geot. Conf., 17th – 19th Dec. 2015, Pune, Maharashtra, India

Lee J-S, Dodds J, Santamarina JC (2007) Behavior of Rigid-Soft Particle Mixtures. Journal of Materials in Civil Engineering, Vol. 19, No. 2, February 1:179-184

Lee JH, Salgado R, Bernal A, Lovell CW (1999) Shredded tires and rubber-sand as lightweight backfill. J. Geot. and Geoenv. Eng., 125(2):132–141.

Lings ML, Greening PD (2001) A novel bender/extender element for soil testing. Geotechnique, 51(8):713-717

McCartney JS, Ghaaowd I, Fox PJ, Sanders MJ, Thielmann SS, Sander AC (2017) Shearing Behavior of Tire-Derived Aggregate with Large Particle Size. II: Cyclic Simple Shear. J. Geot. and Geoenv. Eng., 143 (10 October 2017)

Madhusudhan BR, Boominathan A, Banerjee S (2017) Static and Large-Strain Dynamic Properties of Sand–Rubber Tire Shred Mixtures. Journal of Materials in Civil Engineering. 29(10): 04017165, doi: 10.1061/(ASCE)MT.1943-5533.0002016

Madhusudhan BR, Boominathan A, Banerjee S (2019) Factors Affecting Strength and Stiffness of Dry Sand-Rubber Tire Shred Mixtures. Geotech Geol Eng, 37:2763-2780. https://doi.org/10.1007/s10706-018-00792-y

Madhusudhan, B.R., Boominathan, A. and Subhadeep Banerjee. (2018) Comparison of Cyclic Triaxial Test Results on Sand-Rubber Tire Shred Mixtures with Dynamic Simple Shear Test Results Geotechnical Earthquake Engineering and Soil Dynamics V, June 10–13, Austin, Texas, https://doi.org/10.1061/9780784481486.014

Mashiri MS, Vinod JS, Sheikh MN (2016) Liquefaction Potential and Dynamic Properties of Sand-Tyre Chip (STCh) Mixtures. Geot. Test. J., 39(1):69–79.

Millen, M., Rios, S., Quintero, J., & Viana da Fonseca, A. (2019). Prediction of time of liquefaction using kinetic and strain energy. Soil Dynamics and Earthquake Engineering. DOI: 10.1016/j.soildyn.2019.105898

Nakhaei A, Marandi SM, Kermani SS, Bagheripour MH (2012) Dynamic properties of granular soils mixed with granulated rubber. Soil Dyn. Earthq. Eng., 43:124–132.

Özkul ZH, Baykal G (2007) Shear Behavior of Compacted Rubber Fiber-Clay Composite in Drained and Undrained Loading. J. Geotech. Geoenviron. Eng., 133(7):767–781

Pistolas GA, Anastasiadis A, Pitilakis K (2018) Dynamic Behaviour of Granular Soil Materials Mixed with Granulated Rubber: Effect of Rubber Content and Granularity on the Small-Strain Shear Modulus and Damping Ratio. Geotech Geol Eng, 36:1267-1281

Pradelok S, Łupieżowiec M (2017) Vibration propagation in subsoil: in-situ testing and numerical analyses. Architecture Civil Engineering Environment, 2017, 10.1.:79-86

Richart FE, Hall JR, Woods RD (1970) Vibrations of Soils and Foundations. Prentice Hall, Englewood Cliffs, 414 pp.

Seda JH, Lee JC, Carraro JAH (2007) Beneficial Use of Waste Tire Rubber for Swelling Potential Mitigation in Expansive Soils. Geotechnical Special Publication 172, American Society of Civil Engineers, Denver:1–9.

Soares M (2015) Evaluation of soil liquefaction potential based on laboratory data. Major factors and limit boundaries. PhD thesis, University do Porto

Stempkowska A (2014) Properties of clays and clinkers. Red Clay. Report, AGH University of Science and Technology, Kraków (in Polish)

Szczepański T (2017) Saturating overconsolidated cohesive soils: theory and standards versus reality. 6th Int Worksh. In situ and lab characterization of OC subsoil, Poznań:93-100

Shariatmadari N., Karimpour-Fard M., and Shargh A. (2018). Undrained monotonic and cyclic behavior of sand-ground rubber mixtures. Earthquake engineering and engineering vibration, 17: 541-553, https://doi.org/10.1007/s11803-018-0461-x

Tatlisoz N, Edil TB, Benson CH (1998) Interaction between reinforcing geosynthetics and soil-tire chip mixtures. J. Geotech. Geoenviron. Eng., vol. 124, 11:1109-119

Teixeira S (2015) Evaluation and modelling of sandy soil behavior in terms of liquefaction potential. MSc thesis, University of Porto (in Portuguese).

Thompson DJ, Jiang J, Toward M, Hussein M, Ntotsios E, Dijckmans A, Coulier P, Lombaert G, Degrande G (2016) Reducing railway-induced ground-borne vibration by using open trenches and soft-filled barriers. Soil Dyn. Earthq. Eng. 88:45–59

Trifunac MD (2003) Nonlinear Soil Response as a Natural Passive Isolation Mechanism. Paper II. The 1933, Long Beach, California Earthquake, Soil Dyn. Earthquake Engrg., Vol. 23, No. 7:549-562.

Tsang H-H, Lo SH, Xu X, Sheikh MN (2012) Seismic isolation for low-to-medium-rise buildings using granulated rubber–soil mixtures: numerical study. Earthq. Eng. Struct. Dyn., 41:2009–2024.

Tsang H-H, Pitilakis K (2019) Mechanism of geotechnical seismic isolation system: Analytical modeling. Soil Dyn. Earthq. Eng., 122:171-184

Valle-Molina, C., Stokoe, K. (2012). Seismic measurements in sand specimens with varying degrees of saturation using piezoelectric transducers. Canadian Geotechnical Journal, 49, 671-685, doi:10.1139/T2012-033

Vieira N, Viana da Fonseca A, Ferreira C (2005) Proceso de saturación de ensayos triaxiales. Geotecnia, 104, 31-42, Sociedade Portuguesa de Geotecnia (in Spanish)

Vinot V, Baleshwar S (2013) Shredded tire-sand as fill material for embankment applications. J. Env. Res. and Dev., 7(4A), April - June 2013:1622-1627.

Watanabe K, Kusakabe O (2013) Reappraisal of loading rate effects on sand behavior in view of seismic design for pile foundation. Soils Found., 53(2): 215–231

Yamada Y, Ishihara K (1979) Anisotropic deformation characteristics of sand under three-dimensional stress conditions. Soils and Foundations, 19(2):79-94

Yoon S, Prezzi M, Siddiki NZ, Kim B (2005) Construction of test embankment using sand-tire shred mixture as fill material. Waste Management, 26:1033 – 1044.

Youwai S, Bergado DT (2003) Strength and deformation characteristics of shredded rubber tire - sand mixtures. Canadian Geotechnical Journal, 40:254–264.

**TABLES**

**Table 1.** Properties of the studied soils

| Coimbra Sand | | Red Clay | |
|---|---|---|---|
| Specific gravity | 2.60 | Specific gravity | 2.72 |
| Minimum void ratio (ASTM, 2016) | 0.48 | Liquid limit (*LL*) (CEN, 2009: cone penetration) | 45% |
| Maximum void ratio (ASTM, 2016a) | 0.81 | Plastic limit (*PL*) | 16% |
| Mean effective diameter ($D_{50}$) | 0.35 mm | Plasticity index (*IP*) | 29% |
| Uniformity coefficient ($C_u$) | 2.0 | Mean effective diameter ($D_{50}$) | 0.0033 mm |
| Curvature coefficient ($C_c$) | 0.97 | Clay content | 33% |
| Unified Classification (ASTM, 2011) | Poorly graded sand (SP) | Unified Classification (ASTM, 2011) | Lean clay (CL) |

**Table 2.** Parameters of Crumb Rubber (Biosafe)

| Parameters | Test method | Results |
|---|---|---|
| Colour | Visual | black |
| Bulk density (uncompacted) | ISO (2015) | 0.35 ± 0.02 |
| Specific gravity | Helium pycnometer (ASTM C604-02, 2012) | 1.15 ± 0.06 |
| Moisture (% weight) | Internal | < 1.0 |
| Steel particles | CEN TS 14243 (2010) | < 0.1 |
| Textile fibre particles (% weight) | CEN TS 14243 (2010) | < 0.1 |
| Inerts (% weight) | CEN TS 14243 (2010) | < 1.0 |
| Surface area [$cm^2$/g] | ASTM B922 (2010) Brunauer, Emmett and Teller Theory (B.E.T.) | 620 ± 40 |
| Dimensions [mm] | CEN TS 14243 (2010) | 0.01 - 0.08 |
| Mean effective diameter ($D_{50}$) [mm] | - | 0.44 |
| Uniformity coefficient ($C_u$) | ISO (2004) | 2.67 |
| Curvature coefficient ($C_c$) | ISO (2004) | 1.47 |

**Table 3.** Summary of triaxial tests

| Soil | Test name | Type of equipment [a)] | $D$ (mm) [b)] | $G_s^{Mix}$ (-) | $B$ (-) | Conditions at moulding stage $w$ (%) | Conditions at moulding stage $e$ (-) |
|---|---|---|---|---|---|---|---|
| Coimbra sand (CS) | CS_9 | BW cell | 50 | 2.33 | 1.00 | 4.56 | 0.88 |
| | CS_9_CT | CTx cell | 70 | | 1.00 | 5.40 | 0.62 |
| | CS_33 | BW cell | 50 | 1.83 | 1.00 | 3.44 | 0.86 |
| | CS_33_CT | CTx cell | 70 | | 1.00 | 4.59 | 0.67 |
| Red Clay (RC) | RC_0 | BW cell | 50 | 2.72 | 0.94 | 18.80 | 0.69 |
| | RC_9 | BW cell | 50 | 2.42 | 0.90 | 18.28 | 0.56 |
| none | R_100 | BW cell | 50 | 1.15 | 0.97 | 2.22 | 0.95 |

[a)] BW – Bishop-Wesley's cell, CTx – Conventional triaxial cell with cyclic actuator; [b)] $D$ – specimen diameter

**Table 4.** Loading stages in cyclic tests

| | BW cell | | | Cyclic CTx cell | | |
|---|---|---|---|---|---|---|
| Loading stage | Minimum Load (N) | Maximum load (N) | Frequency (Hz) | Minimum Load (N) | Maximum load (N) | Frequency (Hz) |
| 1 | 0 | 3 | 0.05 | -3 | 3 | 1 |
| 2 | 0 | 6 | 0.03 | -6 | 6 | 1 |
| 3 | 0 | 12 | 0.02 | -12 | 12 | 1 |
| 4 | 0 | 24 | 0.01 | -18 | 18 | 1 |
| 5 | 0 | 48 | 0.005 | -24 | 24 | 1 |
| 6 | 0 | 96 | 0.003 | -36 | 36 | 1 |
| 7 | 0 | 192 | 0.002 | -48 | 48 | 1 |
| 8 | 0 | 384 | 0.001 | -72 | 72 | 1 |
| 9 | | | | -96 | 96 | 1 |
| 10 | | | | -144 | 144 | 1 |
| 11 | | | | -192 | 192 | 1 |

**Table 5.** Number of loading stages before failure in compression-decompression cyclic tests

| Test | Number of loading stages (LS) before failure |
|---|---|
| CS_9 | 5 complete LS + 4 cycles |
| CS_33 | 6 complete LS + 1 cycle |
| RC_0 | 7 complete LS |
| RC_9 | 6 complete LS + 1 cycle |
| R_100 | 7 complete LS + 1 cycle |

**Table 6.** Elastic moduli values determined based on seismic wave velocities

| Test | $\rho$ (g/cm$^3$) | $V_s$ (m/s) | $V_p$ (m/s) | $G_0$ (MPa) | $v$ (-) | $E_0$ (MPa) |
|---|---|---|---|---|---|---|
| CS_0 | 1.94 | 142.11 | 1536.37 | 38.0 | 0.496 | 113.8 |
| CS_9 | 1.82 | 143.45 | 1541.36 | 37.5 | 0.495 | 112.2 |
| CS_33 | 1.51 | 76.45 | 1796.46 | 8.8 | 0.499 | 26.4 |
| RC_0 | 2.51 | 156.32 | 1451.16 | 61.3 | 0.493 | 183.4 |
| RC_9 | 2.42 | 102.79 | 1544.88 | 25.6 | 0.498 | 76.5 |
| R_100 | 0.95 | 55.02 | 1828.26 | 2.9 | 0.499 | 8.6 |

**Table 7.** Conclusions of other researchers in terms of influence of rubber inclusion on damping ratio

| Reference | Material | $\frac{D_{50.rub}}{D_{50.sand}}$ | $R$ [%] | Type of test / confining stress [kPa] / method of specimen preparation | Damping ratio change: at increasing shear strain / at increasing rubber content: |
|---|---|---|---|---|---|
| Anastasiadis et al. (2012) | rubber: $D_{50}$ = 0.35, 0.4, 1.5 & 2.8 mm<br>sands and gravels: $D_{50}$ = 0.27, 0.56, 1.33, 2.9, 3.0 & 7.80 mm | 1, 2, 5, 10 | 0, 5, 10, 15, 25, 35 | RC / 25, 50, 100, 200, 400 kPa / under-compaction, $D_r$ = 91 - 100% | increase / increase, but the effect diminishes at shear strains greater than $10^{-4}$ |
| Ehsani et al. (2015) | rubber: $D_{50}$ = 0.76 mm & 1.78 mm<br>Firoozkooh sand: $D_{50}$ = 0.22 mm | 3.5, 8.2 | 4, 6, 11 | RC & CTx / 300 / compacted at optimum water content | increase / no significant effect |
| Madhusudhan et al. (2017, 2019) | rubber: 0.063 - 2 mm, $D_{50}$ = 1.1 mm<br>sand: $D_{50}$ = 0.6 mm | 1.8 | 0, 10, 30, 50, 100 | CU CTx & CTx on dry samples/ 100 / dry tamping with 70% Proctor energy, $D_r$ = 75 - 80% | increase for sand-rubber mixtures and constant value for rubber-alone / decrease (an exception was the specimen with R = 10% for which D turned out to be greater than for pure sand) |
| Mashiri et al. (2016) | rubber chips:8 x 20 mm<br>sand: $D_{50}$ = 0.35 mm | 14.3 | 0, 10, 20, 30, 40 | CU CTx, $\gamma$ = (1.5 - 5) $\cdot 10^{-3}$ / 69 / dry deposition, $D_r$ = 50% | increase / slight increase |
| Nakhaei et al. (2012) | rubber: 0.15 - 9.5 mm in size, $D_{50}$ = 2 mm<br>well graded fluvial gravel with clay: $D_{50}$ = 4.5 mm | 0.4 | 0, 8, 10, 14 | large-scale CTx / 50, 100, 200, 300 kPa / under-compaction at optimum water content | increase / decrease for $\sigma'_c$ = 50 & 100 kPa, increase for $\sigma'_c$ = 200 & 300 kPa |
| Pistolas et al. (2018) | mix 1: rubber ($D_{50}$ = 1.55 mm) + river sand ($D_{50}$ = 0.41 mm)<br>mix 2: rubber ($D_{50}$ = 3.38 mm) + quarry gravel ($D_{50}$ = 7.14 mm) | 0.5, 4.0 | 0, 10, 15, 20, 40, 60 | RC & CTx / 25, 50, 100, 200 / dry tamping to obtain void ratio e = 0.7, $D_r$ = 45 - 75% (mix 1) & 70% (mix 2) | RC: continuous increase; CTx: decrease for $\gamma$ up to about (3 - 7)$\cdot 10^{-4}$ and then further increase / RC: increase; CTx: decrease |

**FIGURE CAPTIONS**

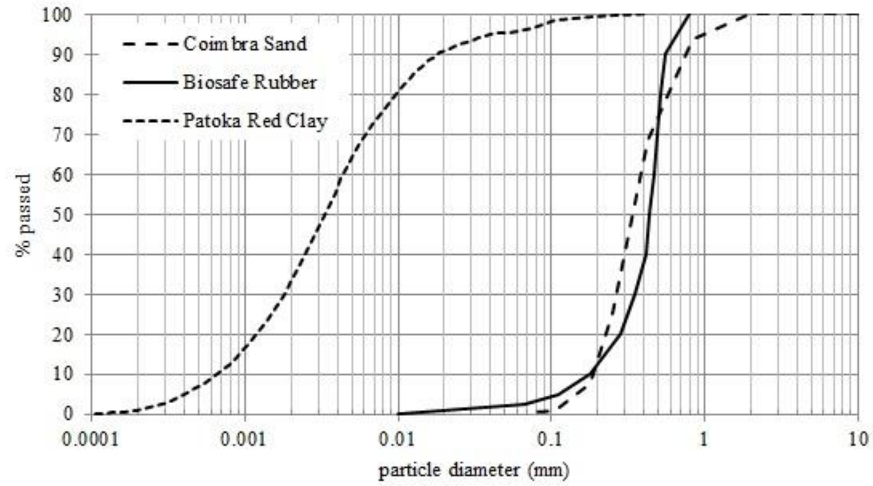


**Fig. 1** Grain size distribution of Coimbra sand, Patoka Red Clay and rubber

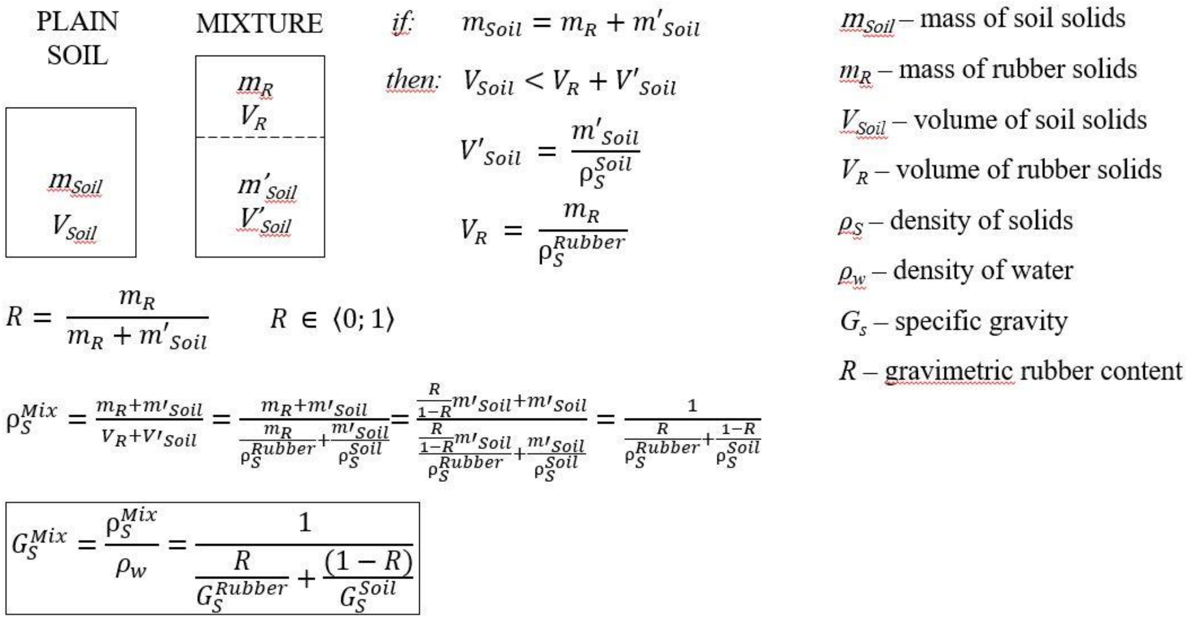


**Fig. 2** Definition of gravimetric rubber content R and specific gravity of soil-rubber mixtures $G_s^{Mix}$

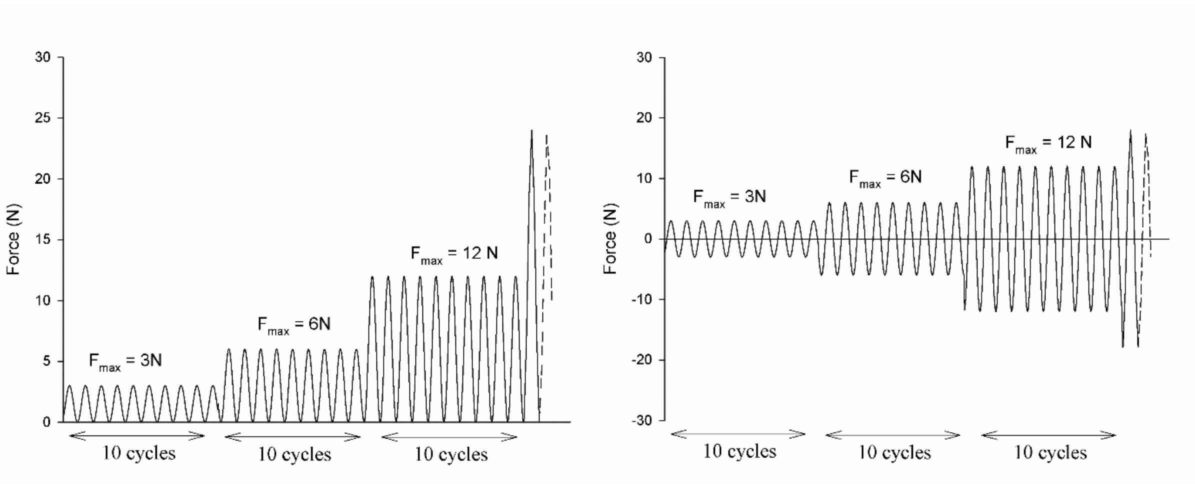


a) b)

**Fig. 3** Scheme of cyclic loading: a) in the BW cell; b) in the cyclic CTx cell

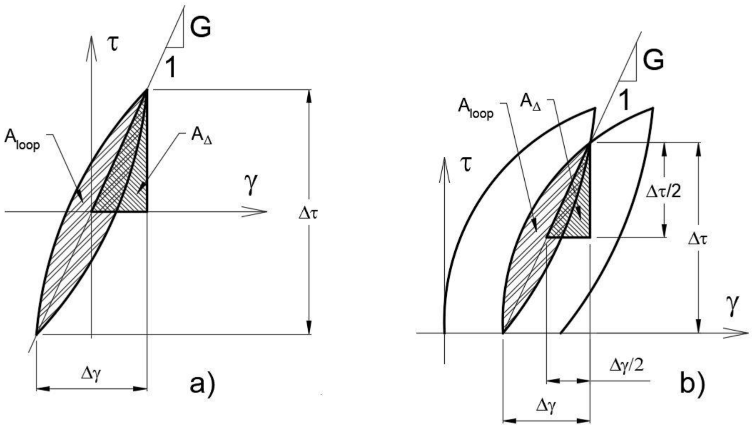


**Fig. 4** Definition of shear modulus and damping ratio – based on τ-γ graph of a: a) cyclic compression – extension test and b) cyclic compression – decompression test

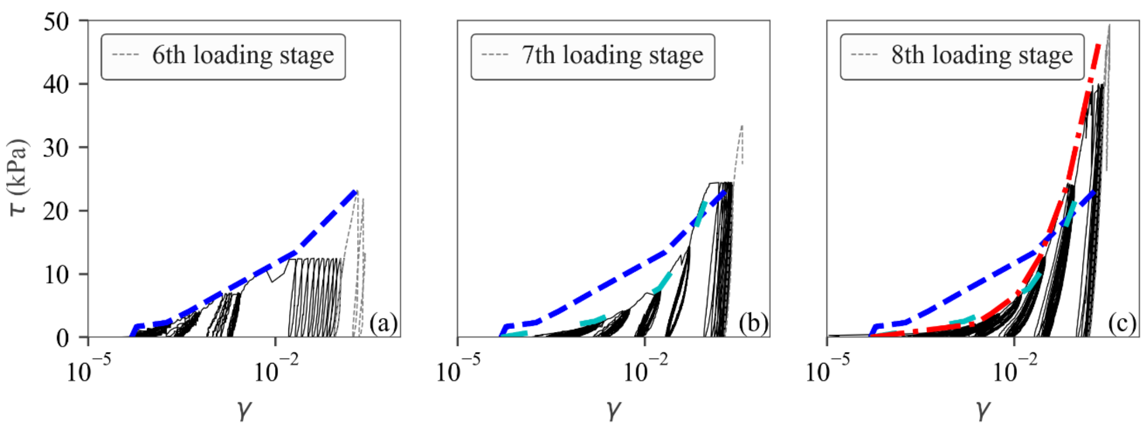


**Fig. 5** Shearing characteristics in cyclic compression – decompression triaxial tests on sand-rubber mixtures and rubber alone: a) CS_9; b) CS_33; c) R_100. Note: The dashed grey line represents the last loading stage while the solid line represents the previous loading stages

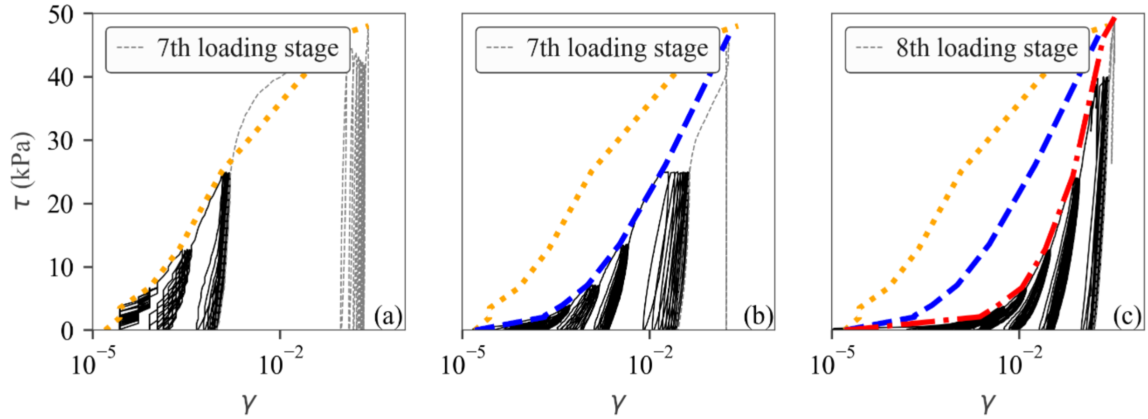


**Fig. 6** Shearing characteristics in cyclic compression – decompression triaxial tests on clay-rubber mixtures and rubber alone: a) RC_0; b) RC_9; c) R_100. Note: The dashed grey line represents the last loading stage while the solid line represents the previous loading stages

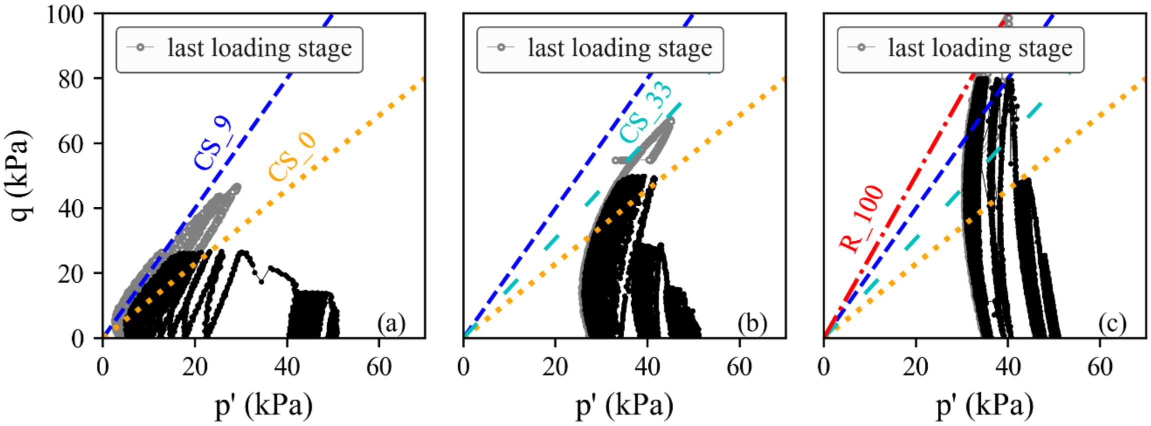


**Fig. 7** Stress paths p’ - q of cyclic compression – decompression triaxial tests on sand-rubber mixtures and rubber alone: a) CS_9; b) CS_33, c) R_100. Note: The grey marker represents the last loading stage while the black markers represent the previous loading stages

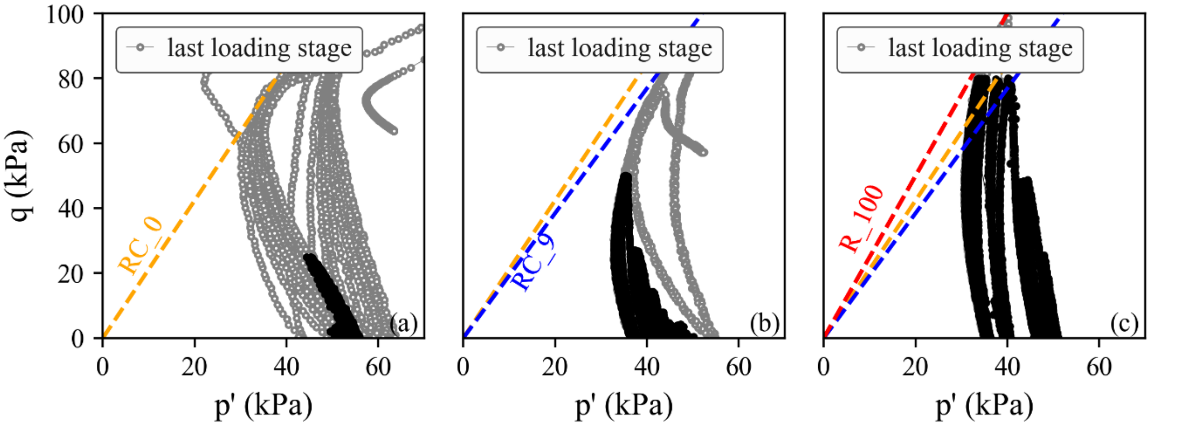


**Fig. 8** Stress paths p’ - q of cyclic compression – decompression triaxial tests on: a) clay RC_0, b) clay-rubber mixture RC_9, c) rubber alone R_100. Note: The grey marker represents the last loading stage while the black markers represent the previous loading stages

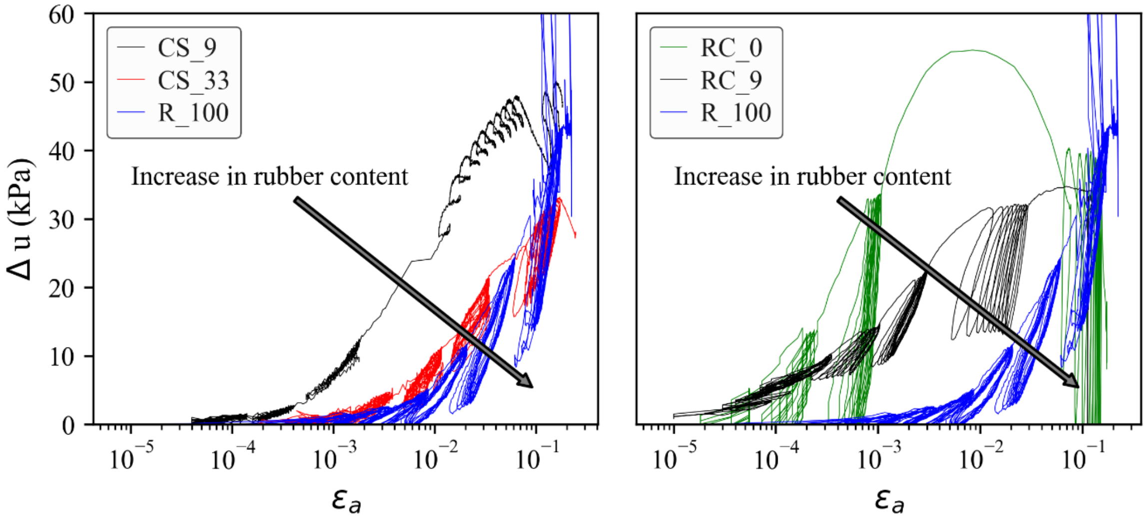


**Fig. 9** Pore pressure evolution in cyclic compression – decompression triaxial tests: a) sand-rubber specimens; b) clay-rubber specimens

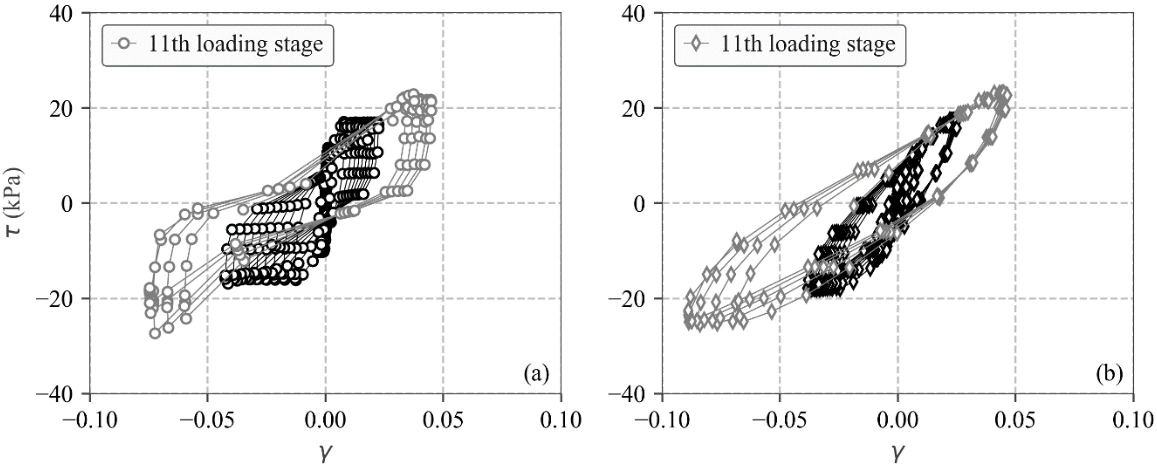


**Fig. 10** Shearing characteristics in cyclic compression – extension triaxial tests on sand-rubber mixtures: a) CS_9_CT; b) CS_33_CT. Note: The grey marker represents the last loading stage while the black markers represent the previous loading stages

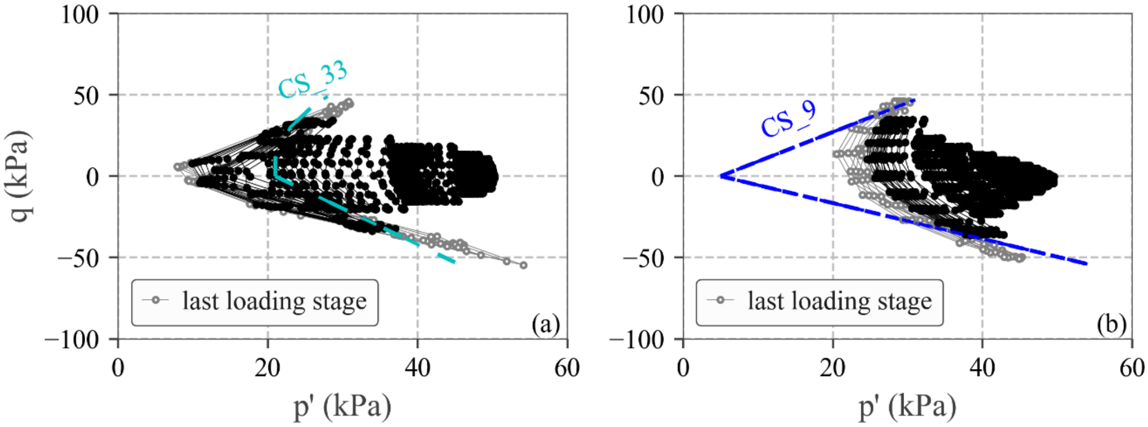


**Fig. 11** Stress paths p' - q of cyclic compression – extension triaxial tests on compacted sand-rubber mixtures: a) CS_9_CT; b) CS_33_CT. Note: The grey marker represents the last loading stage while the black markers represent the previous loading stages

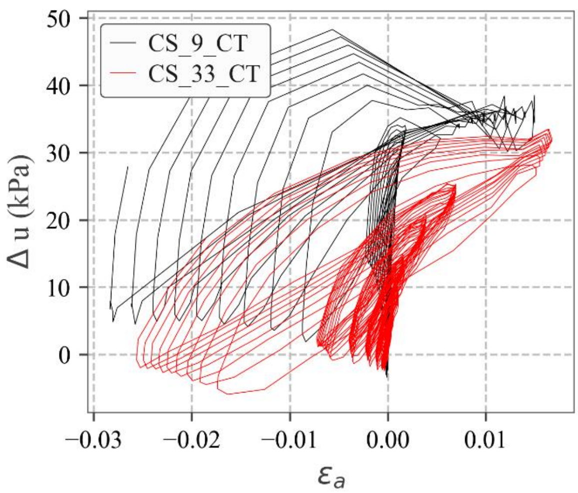


**Fig. 12** Pore pressure evolution in cyclic compression – extension triaxial tests on sand-rubber mixtures

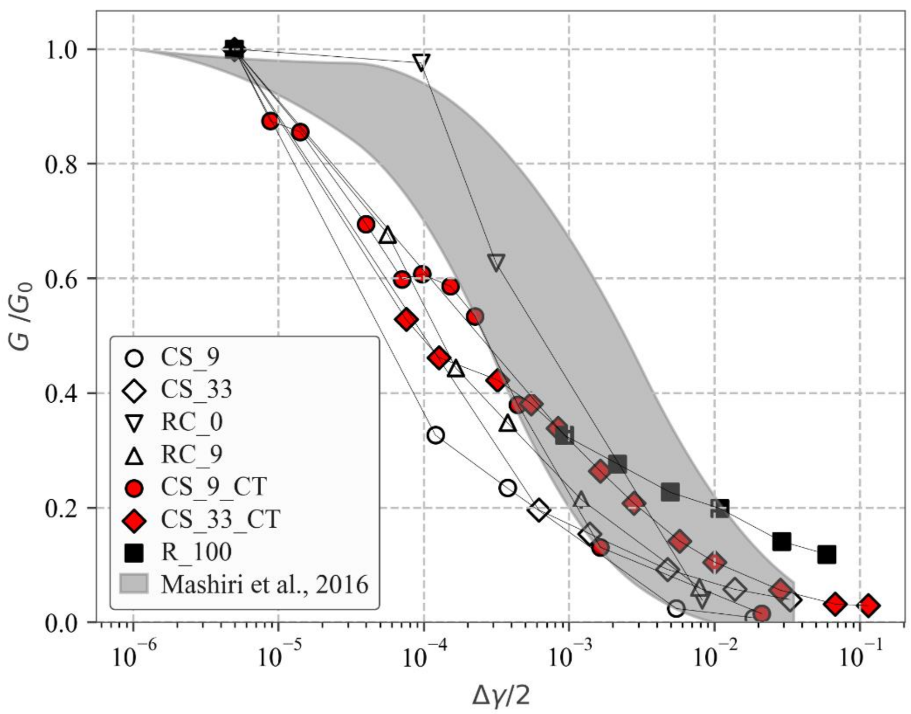


**Fig. 13** Normalized shear moduli of all the mixtures

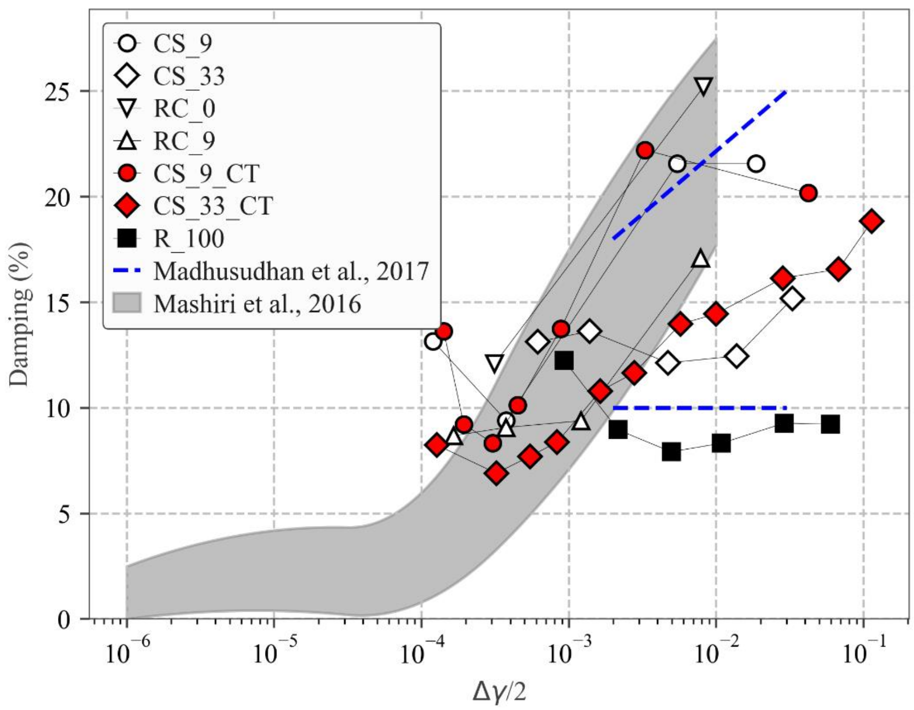


**Fig. 14** Damping ratios of all the mixtures at confining pressure 50 kPa

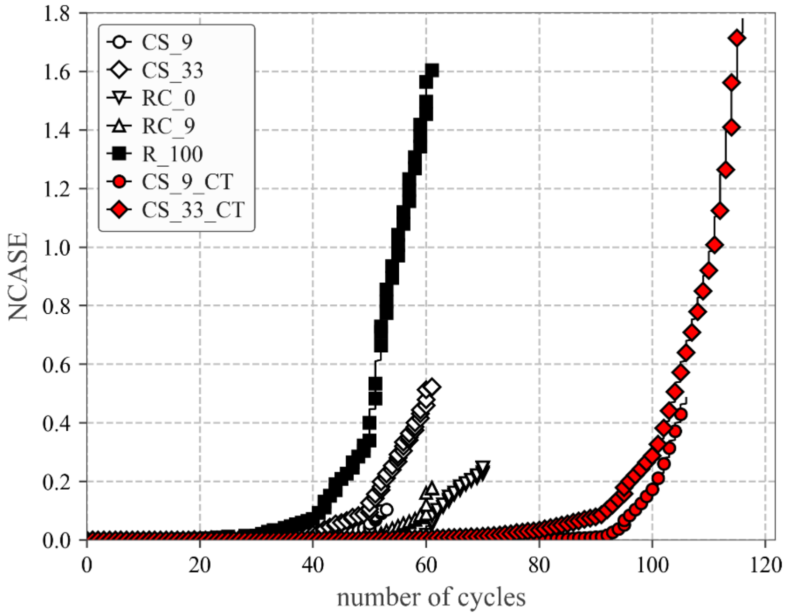


**Fig. 15** Normalized accumulated absolute strain energy, NCASE

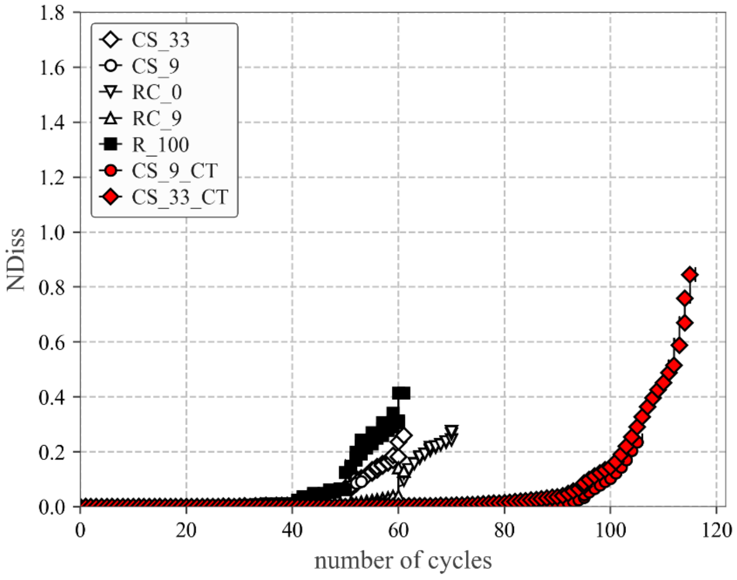


**Fig. 16** Normalized dissipated energy, NDiss